Elucidation of the biosynthetic pathway of reserpine

Jiaqing Cao[1], Jingxiao Zhong[1,2,3], Feng Li[1,4], Yindi Jiang[1,*]

[1] Key Laboratory of Quantitative Synthetic Biology, Shenzhen Institute of Synthetic Biology, Shenzhen Institutes of Advanced Technology, Chinese Academy of Sciences, Shenzhen 518055, China.

[2] School of Life Sciences, Henan University, Kaifeng 475004, China.

[3] Shenzhen Research Institute of Henan University, Shenzhen 518000, China.

[4] University of Chinese Academy of Sciences, Beijing 100049, China.

[*]E-mail: yd.jiang@siat.ac.cn

Abstract

Reserpine is a landmark natural product that has profoundly influenced our understanding of neurotransmitter biology and cardiovascular medicine. Its complex structure, featuring a unique C3 β-configuration and five consecutive chiral centers, has inspired generations of synthetic chemists to develop innovative strategies for its construction. However, the biosynthetic logic underlying nature's assembly of this intricate molecule has remained elusive. Here, we decipher the biosynthetic pathway of reserpine in *Rauvolfia verticillata*, revealing that α-configured strictosidine serves as the biosynthetic precursor. The crucial C3 β-configuration is established through a two-step enzymatic epimerization, orchestrated by a flavin-dependent oxidase and a NADPH-dependent reductase. The consecutive chiral centers are constructed through coordinated action of distinct enzyme families. Through the identification of eight biosynthetic enzymes, including those catalyzing late-stage methoxylation, we successfully reconstituted the biosynthesis of rauvomitorine G, a key intermediate in reserpine formation. This work unveils nature's elegant approach to stereoselective synthesis of complex alkaloids and provides valuable biocatalytic tools for molecular functionalization.

Introduction

Reserpine is a structurally complex monoterpene indole alkaloid (MIA) that has profoundly influenced our fundamental understanding of biomedicine and chemistry. Since its isolation from *Rauvolfia serpentina* in 1952, reserpine has been instrumental for deciphering the complex mechanisms of neurotransmitter storage and release, particularly regarding monoamine neurotransmitters such as serotonin and norepinephrine[1,2,3]. Its ability to deplete these neurotransmitters has provided groundbreaking insights into the pathophysiology of hypertension and various psychiatric disorders[4,5]. Furthermore, reserpine's clinical application as antihypertensive and antipsychotic agents paved the way for the development of more targeted therapeutics, revolutionizing the treatment paradigms in cardiovascular and mental health medicine[6].

Beyond its biomedical significance, the complex structure of reserpine has challenged and inspired generations of synthetic chemists, leading to numerous total syntheses and innovative synthetic methodologies[7]. The molecule's pentacyclic skeleton features a unique C3β stereochemistry and five consecutive chiral centers densely packed in the E ring (Fig. 1a). Most total syntheses of reserpine begin with the construction of a pentasubstituted E-ring, typically achieved through various synthetic strategies including Diels-Alder reaction, double Michael addition, and radical cyclization (Fig. 1b)[8,9,10,11,12]. This elaborated E-ring subsequently undergoes Pictet-Spengler condensation with 6-methoxytryptamine to generate a pentacyclic intermediate bearing an α-configuration at C3. Access to the desired β-configuration at C3 has largely relied on R. B. Woodward's landmark conformational control strategy, which involves locking the molecule in an unfavorable conformation through lactonization, followed by acid treatment to achieve late-stage C3 epimerization[8]. Despite these sophisticated strategies developed by synthetic chemists, the biosynthetic pathway by which nature constructs such complex natural products remains elusive.

Isotope feeding studies have established tryptamine as the biosynthetic precursor of reserpine[13]. Its condensation with monoterpene-derived secologanin yields two diastereomers, vincoside and strictosidine[14]. The shared C3 configuration between vincoside and reserpine has historically

63 suggested vincoside as the biosynthetic precursor of reserpine[7]. However, this proposal contradicts
64 established MIA biosynthetic pathways, where strictosidine, not vincoside, functions as the
65 common precursor[15]. This discrepancy raises an intriguing possibility that strictosidine might serve
66 as the reserpine precursor, necessitating subsequent stereochemical inversion to establish the
67 characteristic C3β configuration of reserpine.
68
69 Here we report the elucidation of the reserpine biosynthetic pathway in *R. verticillata* through an
70 integrated approach combining transcriptome mining, heterologous expression, and biochemical
71 characterization (Fig. 1c and 2). Our findings reveal that strictosidine, not vincoside, serves as the
72 authentic precursor in reserpine biosynthesis. We uncovered the enzymatic basis for C3
73 epimerization in *Rauvolfia*, which proceeds through a two-step process: an FAD-dependent
74 oxidase *Rv*YOO generates an imine intermediate, which is subsequently reduced by a medium-
75 chain dehydrogenase/reductase (MDR) *Rv*DYR1 to yield the 3-epi product. Furthermore, we
76 revealed nature's elegant strategy for constructing consecutive chiral centers in ring E, where two
77 stereocenters are established through stereoselective reduction by an MDR *Rv*YOS, and the final
78 stereocenter is installed via cytochrome P450 monooxygenase *Rv*CYP71D820. Through the
79 identification of eight biosynthetic enzymes, including P450 monooxygenase *Rv*CYP72A270 and
80 *O*-methyltransferase *Rv*11OMT for late-stage methoxylation, we successfully reconstituted
81 rauvomitorine G, a crucial intermediate in reserpine biosynthesis. This work advances our
82 understanding of complex alkaloid biosynthesis, revealing both the enzymatic logic underlying
83 reserpine biosynthesis and providing valuable biocatalytic tools for selective functionalization of
84 complex molecular scaffolds.
85
86 **Results**
87
88 To elucidate the biosynthesis of reserpine, we first examined the distribution of monoterpene
89 indole alkaloids (MIAs) in *Rauvolfia verticillata*, a medicinal plant used in China as a source of
90 reserpine. Liquid chromatography-mass spectrometry (LC-MS) analysis of tissue extracts revealed
91 several key MIAs, including reserpine (**11**), deserpidine (**13**), α-yohimbine (**2**), and 3-epi-α-
92 yohimbine (**4**) (Supplementary Fig. 1). Having confirmed the presence of these MIAs across

93 different tissues, we sought to identify the genes responsible for their biosynthesis. To facilitate
94 biosynthetic gene discovery, we generated tissue-specific transcriptome datasets in triplicate.
95
96 **Formation of α-yohimbine through strictosidine pathway**
97 A distinct structural feature of reserpine is its β-configuration at C3, which contrasts with the α-
98 configuration predominant in most MIAs. The isolation of vincoside and vincoside lactam, which
99 share this β-configuration at C3, from *Rauvolfia* species has long suggested vincoside as the
100 biosynthetic precursor of reserpine (Supplementary Fig. 2)[7,16]. However, the stepwise conversion
101 from vincoside to reserpine remains unsolved.
102
103 Strictosidine (**1**), a stereoisomer of vincoside and the common MIA precursor, is stereospecifically
104 synthesized from tryptamine and secologanin by strictosidine synthase (STR). The subsequent
105 deglycosylation by strictosidine glucosidase (SGD) generates a reactive iminium intermediate,
106 which various reductases can transform into diverse indole alkaloids[15]. While *Rauvolfia* SGD
107 showed specificity for **1** deglycosylation, it exhibits no activity towards vincoside[17]. Notably,
108 *Catharanthus roseus* SGD (*Cr*SGD) can deglycosylate both **1** and vincoside, suggesting the
109 possible existence of an unidentified vincoside-specific SGD in *Rauvolfia*[18].
110
111 The prevalence of C3 β-configured intermediates in *Rauvolfia* is evidenced by numerous isolated
112 compounds, including vincoside lactam, 3-epi-α-yohimbine (**4**), rauvomitorine G (**9**), deserpidic
113 acid methyl ester (**12**), and rescinnamine, with **4** representing the structurally simplest intermediate
114 (Supplementary Fig. 2)[19,20,21]. Recent studies have elucidated the biosynthesis of α-yohimbine (**2**),
115 the C3 epimer of **4**, in *R. tetraphylla*[22]. This pathway proceeds via strictosidine (**1**), involving SGD-
116 catalyzed formation of a reactive imine intermediate and subsequent reduction by yohimbane
117 synthase (YOS), a medium-chain dehydrogenase/reductase (MDR).
118
119 These findings led us to propose two potential biosynthetic pathways for 3-epi-α-yohimbine (**4**)
120 (Supplementary Fig. 3). Pathway A involves condensation of tryptamine and secologanin to form
121 vincoside (**1a**), followed by conversion to **4** through an unidentified SGD and an MDR.
122 Alternatively, pathway B begins with STR-mediated condensation of tryptamine and secologanin
123 to produce strictosidine (**1**)[23], which is converted to α-yohimbine (**2**) by characterized SGD and

124 YOS enzymes[22,24]. Subsequently, stereochemical inversion of C-3 of **2** could be catalyzed by an
125 unidentified epimerase to yield **4**.
126
127 To investigate pathway A, we chemically synthesized a mixture of strictosidine (**1**) and vincoside
128 (**1a**). Five putative candidate genes potentially capable of vincoside deglycosylation were
129 identified in the *R. verticillata* transcriptome using *Cr*SGD as a query. Each gene was cloned from
130 *R. verticillata* cDNA and expressed in *Nicotiana benthamiana*. LC-MS analysis revealed that
131 while *Rv*SGD1 effectively consumed strictosidine (**1**), vincoside remained unchanged in all SGD
132 candidate assays (Supplementary Fig. 4), suggesting that vincoside is not the source of 3-*epi*-α-
133 yohimbine (**4**).
134
135 We then explored pathway B through reconstituting α-yohimbine (**2**) in planta (Fig. 3a). Previous
136 work in *R. tetraphylla* showed that YOS reduces strictosidine aglycone to form a mixture of
137 yohimbine-type alkaloids, including α-yohimbine (**2**), yohimbine (**2a**), and corynanthine (**2c**)[22].
138 BLAST analysis of the *R. verticillata* transcriptome using *Rt*YOS as a query revealed a candidate
139 gene, *Rv*YOS, sharing 94.4% sequence identity. To assess functional conservation, we
140 coexpressed *Rv*YOS with *Catharanthus roseus* STR (*Cr*STR) and *Rv*SGD in *N. benthamiana*.
141 Following infiltration of tryptamine and secologanin, this system successfully produced both **2** and
142 **2a** (Supplementary Fig. 5). The formation of these products was further confirmed *in vitro* using
143 purified *Cr*STR, *Rv*SGD, and *Rv*YOS enzymes (Supplementary Fig. 5). Although *Rv*YOS
144 generated **2**, its lack of product specificity led us to screen all MDRs sharing over 30% sequence
145 identity for enzymes that could selectively produce **2** (Fig. 3b). As none exhibited the desired
146 specificity, we proceeded with a chemical standard of **2** for subsequent experiments.
147
148 **Enzymatic epimerization of α-yohimbine (2)**
149 We next investigated the enzymatic basis of α-yohimbine (**2**) epimerization to 3-epi-α-yohimbine
150 (**4**). Epimerization could be catalyzed by epimerases, which are crucial in the primary metabolism
151 of carbohydrates and amino acids, as well as in secondary metabolite biosynthesis[25,26]. During
152 morphine biosynthesis in opium poppy, a reticuline epimerase (REPI) catalyzed the
153 stereoconversion of *S*-reticuline to *R*-reticuline through sequential oxidation and reduction with its
154 two domains[27]. The N-terminal cytochrome P450 domain oxidizes *S*-reticuline to an iminium

155 intermediate, which was stereo-specifically reduced by the C-terminal aldo-keto reductase (AKR)
156 domain to *R*-reticuline in a NADPH-dependent manner (Supplementary Fig. 6). Thus, we
157 speculated that epimerization of α-yohimbine (**2**) happened in a similar manner that **2** was oxidized
158 to iminium intermediate 3-dehydro-α-yohimbine (**3**), followed by reduction from the convex face
159 to give 3-epi-α-yohimbine (**4**) (Fig. 3a).
160
161 Our search for REPI homologs in the *R. verticillata* transcriptome failed to identify candidates
162 containing both P450 and AKR domains. Although the CYP450 domain in REPI belongs to the
163 CYP82 family, expression of seven CYP82 gene candidates from *R. verticillata* in *N. benthamiana*
164 leaves co-infiltrated with **2** yielded no detectable oxidized products. We then considered
165 alternative oxidases other than cytochrome P450s. In vinblastine biosynthesis in *C. roseus*, the
166 flavin-dependent precondylocarpine acetate synthase (*Cr*PAS) oxidizes the tertiary amine in
167 stemmadenine acetate to an iminium intermediate[28]. This led us to investigate PAS homologs as
168 potential oxidants for **2**. Among eight *Cr*PAS homologs identified in the *R. verticillata*
169 transcriptome, one candidate sharing 58.0% identity with *Cr*PAS, which we named α-yohimbine
170 oxidase (*Rv*YOO), catalyzed the conversion of **2** to a product with an exact mass of $[M+H]^+$
171 353.1857, consistent with an oxidized product of **2** (calculated for $C_{21}H_{25}N_2O_3^+$: 353.1860) (Fig.
172 3c). The structure was confirmed using synthetic 3-dehydro-α-yohimbine (**3**), which showed
173 identical retention time, exact mass, and MS/MS fragmentation patterns (Supplementary Fig. 7).
174 Further investigation of *Rv*YOO's substrate scope through in planta expression and infiltration
175 with α-yohimbine stereoisomers revealed that α-yohimbine (**2**), yohimbine (**2a**), and *β*-yohimbine
176 (**2b**) were oxidized, while corynanthine (**2c**) and 3-epi-α-yohimbine (**4**) were not substrates
177 (Supplementary Fig. 7). Notably, the inability of *Rv*YOO to oxidize **4** suggests that once formed,
178 **4** cannot be coverted back to **3** through the same enzymatic mechanism, indicating the irreversible
179 nature of this transformation.
180
181 For the subsequent reduction of 3-dehydro-α-yohimbine (**3**), we focused on MDR enzymes, which
182 are known to catalyze iminium reduction in MIA biosynthesis[29,30,31,32]. A well-characterized
183 example is tetrahydroalstonine synthase (THAS) in *C. roseus* that performs 1,2-reduction of
184 iminium strictosidine aglycone to yield tetrahydroalstonine[33]. Co-expression of either of the two
185 3-dehydro-α-yohimbine reductases (*Rv*DYR1 and *Rv*DYR2) with *Rv*YOO in *N. benthamiana*

186 infiltrated with α-yohimbine (**2**) resulted in the formation of a product that co-eluted with authentic
187 3-epi-α-yohimbine (**4**) standard (Fig. 3d). However, due to incomplete substrate conversion by
188 *Rv*YOO, we observed a mixture of **2** and **4** in *N. benthamiana* leaves expressing active MDRs,
189 which prevented definitive conclusions about the stereoselectivity of *Rv*DYR1 and *Rv*DYR2
190 toward **3**.
191
192 To unambiguously determine stereoselectivity, we expressed and purified N-terminal His6-tagged
193 *Rv*DYR1 and *Rv*DYR2 for *in vitro* characterization (Supplementary Fig. 8). Incubation of
194 synthetic **3** with purified enzymes and NADPH predominantly yielded 3-epi-α-yohimbine (**4**) over
195 α-yohimbine (**2**) (Fig. 3e). Notably, **2** could be generated by NADPH alone, while the formation
196 of **4** required both NADPH and active *Rv*DYR enzymes, indicating *Rv*DYR enzymes' preference
197 for C3β stereoselectivity. Interestingly, despite high sequence similarity among *Rv*DYR1,
198 *Rv*DYR2, and *Rv*DYR15260, *Rv*DYR15260 showed no activity toward the substrate
199 (Supplementary Fig. 9). This lack of activity might be attributed to certain non-conserved residues
200 among these three enzymes. While we were preparing this manuscript, two independent studies
201 reported similar epimerization mechanisms for MIAs in plants[34,35]. To further understand the
202 molecular basis of substrate recognition and and stereochemical control, structural studies
203 including X-ray crystallography and site-directed mutagenesis are currently underway.
204
205 **Stereospecific C18 hydroxylation establishing the fifth chiral center in ring E**
206 The next stage of reserpine biosynthesis involves two hydroxylation events at C11 and C18 as well
207 as two methylation events at O11 and O17. The isolation of 18β-hydroxy-3-epi-α-yohimbine (**5**)
208 and rauvomitorine G (**9**) from *Rauvolfia* suggested that stereospecific hydroxylation at C18 of **4**
209 occurs first, followed by methoxylation at C11 (Fig. 4a)[19,20]. Given that no C18 hydroxylase has
210 been previously reported, sequence homology-based approaches were not feasible for identifying
211 the responsible enzyme. Therefore, we employed a co-expression analysis strategy using *Rv*DYR1
212 as a bait, as the expression of upstream biosynthetic genes showed similar tissue-specific
213 expression patterns and high correlation (Fig. 4b and 4c). We selected 30 P450 enzymes (Pearson's
214 r>0.7) for functional characterization (Supplementary Fig 10). Transient expression of
215 *Rv*CYP71D820 in *N. benthamiana* leaves infiltrated with **4** resulted in the formation of a new
216 product with an exact mass (*m/z* $[M+H]^+$ = 371.1963) matching hydroxylated **4** (calculated for

217 $C_{21}H_{27}N_2O_4^+$: 371.1965) (Fig. 4d). We validated this finding *in vitro* using *Rv*CYP71D820 in yeast
218 microsomal fractions, which efficiently converted **4** to the same product observed in planta (Fig.
219 4d). MS/MS analysis of this product revealed an intact indole moiety (*m/z* $[M+H]^+$ = 144.0807)
220 (Supplementary Fig. 11), indicating hydroxylation occurred outside the indole ring. The product's
221 identity was confirmed using a chemically synthesized standard of **5**, prepared from deserpidine
222 (**13**) in two steps, which showed identical retention time, exact mass, and MS/MS fragmentation
223 patterns (Supplementary Fig. 11). These results establish *Rv*CYP71D820 as the enzyme
224 responsible for stereospecific C18 hydroxylation of **4**, completing the construction of five
225 consecutive chiral centers in the E ring of reserpine.
226
227 **Enzymatic late-stage methoxylation**
228 We next sought to identify the oxidase and methyltransferase responsible for C11 methoxylation
229 of **5**. During vindoline biosynthesis in *C. roseus*, tabersonine 16-hydroxylases (T16Hs) of the
230 CYP71D family catalyze C16 hydroxylation of tabersonine to form 16-hydroxytabersonine,
231 followed by *O*-methylation catalyzed by 16-hydroxytabersonine 16-*O*-methyltransferase (16OMT)
232 to complete methoxy group installation[36,37,38]. Given that the C16 position of tabersonine is
233 structurally equivalent to the C11 position in reserpine, we searched for T16H and 16OMT
234 homologs in the *R. verticillata* transcriptome. When T16H homologs proved inactive toward **5**, we
235 rescreened P450 candidate genes co-expressed with *Rv*DYR1. Among these candidates,
236 coexpression of *Rv*CYP72A270 with *Rv*CYP71D820 in *N. benthamiana* leaves infiltrated with **4**
237 resulted in a product that co-eluted with synthetic 11,18β-dihydroxy-3-epi-α-yohimbine (**6**) (Fig.
238 4e and Supplementary Fig. 12). Next, screening of 16OMT homologs in *N. benthamiana* leaves
239 infiltrated with **6** revealed that only *Rv*11OMT could catalyze the formation of rauvomitorine G
240 (**9**) (Fig. 4d and Supplementary Fig. 13). We further validated this activity using purified N-
241 terminal His6-tagged *Rv*11OMT *in vitro* (Fig. 4f). Finally, co-expression of *Rv*CYP71D820,
242 *Rv*CYP72A270, and *Rv*11OMT in *N. benthamiana* leaves treated with **4** successfully yielded **9**
243 (Fig. 4g), confirming the sequential activities of these enzymes in the pathway.
244
245 **Branched pathway**
246 During the co-expression of *Rv*CYP72A270 and *Rv*CYP71D820 in *N. benthamiana* infiltrated
247 with **4**, we observed a minor peak sharing the exact mass with **5** but exhibiting a different retention

248 time (Supplementary Fig. 14). MS/MS analysis of the peak indicated hydroxylation on the indole
249 ring (Supplementary Fig. 14). Given *Rv*CYP72A270's C11 hydroxylation activity on **5**, we
250 proposed that *Rv*CYP72A270 could also oxidize **4** to form the 11-hydroxy-3-epi-α-yohimbine (**7**).
251 This hypothesis was confirmed when we detected **7** in *N. benthamiana* expressing *Rv*CYP72A270
252 and treated with **4** (Supplementary Fig. 15). Based on *Rv*11OMT's known ability to methylate the
253 C11 hydroxyl group of **6**, we investigated its activity toward **7**. Co-expression of *Rv*CYP72A270
254 and *Rv*11OMT in *N. benthamiana* infiltrated with **4** yielded a product peak (**8**) corresponding to
255 the methoxylated derivative (Supplementary Fig. 15). The MS/MS fragmentation pattern of **8**
256 confirmed the presence of a methoxy group on the indole ring (Supplementary Fig. 15). However,
257 without authentic standards for **7** and **8**, their exact structures could not be unambiguously
258 confirmed. Furthermore, whether **8** could serve as a substrate for *Rv*CYP71D820 to generate **9**
259 remain to be determined. These findings suggest a potential branched pathway from **4** to **9**, adding
260 another layer of complexity to the biosynthetic route (Supplementary Fig. 16).
261
262 **Remaining biosynthetic steps**
263 According to our biosynthetic hypothesis, the next step involves the *O*-methylation of the C17
264 hydroxyl group of rauvomitorine G (**9**) to yield reserpic acid methyl ester (**10**) (Fig. 2). Guided by
265 the robust co-expression patterns observed among our newly identified biosynthetic genes (Fig.
266 4b and 4c), we initially employed co-expression analysis to identify the putative C17 *O*-
267 methyltransferase. We heterologously expressed 30 methyltransferases that showed strong co-
268 expression correlation (r>0.5) with *Rv*11OMT in *N. benthamiana*, using **9** as the substrate.
269 However, none of these candidates exhibited the desired methyltransferase activity. Further
270 exploration of the *R. verticillata* transcriptome for homologs of well-characterized
271 methyltransferases from the MIA biosynthetic pathway, including *Cr*16OMT and loganic acid *O*-
272 methyltransferase (LAMT), also proved unsuccessful (Supplementary Fig. 17)[38,39]. No activity
273 was detected toward either **9** or 18β-hydroxy-3-epi-α-yohimbine (**5**), the latter being a potential
274 substrate for C17 *O*-methylation in the biosynthesis of deserpidine (**13**), a demethoxylated
275 reserpine derivative with significant biological activities[40]. This challenging identification might
276 be attributed to the unique nature of the C17 hydroxyl group of **9**. Typical plant *O*-
277 methyltransferases target hydroxyl groups with relatively lower pKa values, such as phenolic
278 hydroxyl or carboxyl groups[41]. However, the C17 hydroxyl group in **9** has a significantly higher

279 pKa, making it less prone to form oxyanions for nucleophilic attack on *S*-adenosylmethionine.
280 This distinctive property suggest that an unusual methyltransferase might be required to facilitate
281 the deprotonation and subsequent methylation of this challenging hydroxyl group.
282
283 The final step of reserpine biosynthesis involves the transfer of a 3,4,5-trimethoxybenzoyl (TMB)
284 group to reserpic acid methyl ester (**10**) (Fig. 2). Such acylation steps are typically catalyzed by
285 two enzyme families: BAHD-acyltransferases (BAHD-ATs) and serine carboxypeptidase-like
286 acyltransferases (SCPL-ATs)[42]. Recent studies of leonurine biosynthesis in two *Leonurus* species
287 have demonstrated that 4-hydroxy-3,5-dimethoxybenzoic acid (syringic acid) is first glycosylated
288 by a UDP-glucosyltransferase (UGT) to form the glucose ester of syringic acid, which then
289 undergoes SCPL-catalyzed acylation with 4-guanidinobutanol to yield leonurine (Supplementary
290 Fig. 18)[43]. Given the structural similarity between syringic acid and TMB, we hypothesized that a
291 similar pathway operates in reserpine (**11**) biosynthesis, where a UGT glycosylates 3,4,5-
292 trimethoxybenzoic acid (TMBA) to form 1-*O*-TMB-β-D-glucopyranoside (TMB-Glc), followed
293 by SCPL-mediated acylation of **10** (Supplementary Fig. 18).
294
295 To identify the UGT responsible for TMBA glycosylation, we performed transcriptome analysis
296 using the *Leonurus* UGT sequence as a query and identified seven UGT candidate genes
297 (Supplementary Fig. 19). These candidates were cloned from *R. verticillata* cDNA and
298 heterologously expressed in *E. coli* BL21. In vitro assays with purified candidate enzymes, TMBA,
299 and uridine diphosphate glucose (UDP-Glc) revealed that *Rv*UGT1 and *Rv*UGT2 catalyzed TMBA
300 glycosylation, yielding a product identical to the synthetic TMB-Glc standard in retention time,
301 exact mass, and MS/MS fragmentation pattern (Supplementary Fig. 20).
302
303 For the final acylation step, we identified 15 SCPL candidate genes from the transcriptome using
304 the *Leonurus* SCPL sequence as a query (Supplementary Fig. 21). These candidates possessed the
305 characteristic N-terminal signal peptides typical of SCPLs, which require precise post-translational
306 processing for activation (Supplementary Fig. 22). Despite coexpressing full-length versions of
307 each SCPL candidate with *Rv*UGT1 in both *S. cerevisiae* and *N. benthamiana*, reserpine (**11**)
308 formation was not detected when supplementing with reserpic acid methyl ester (**10**) and TMBA.
309 This lack of activity likely stems from the complex post-translational modifications required for

310 SCPL maturation, including signal peptide cleavage, protein folding in the endoplasmic reticulum,
311 and potential glycosylation[42,44]. These plant-specific processing events may not be adequately
312 reproduced in heterologous hosts, suggesting the need for optimized expression conditions or
313 alternative expression systems that better mimic the native cellular environment.
314
315 **Reconstitution of rauvomitorine G (9)**
316 Having identified all biosynthetic enzymes responsible for the production of reserpine biosynthetic
317 intermediate **9**, we aimed to reconstitute **9** in tobacco. We overexpressed eight genes starting from
318 STR to *Rv*11OMT in tobacco and supplemented tryptamine and secologanin as substrates. LC-MS
319 analysis revealed only trace amounts of **3**, **4, 5** and **9** (Fig. 5a). The production efficiency of **9** was
320 significantly compromised likely by the extensive length of the biosynthetic pathway and low
321 efficiency of certain enzymes, particularly *Rv*YOS, which exhibits low catalytic activity and
322 generates multiple yohimbine isomers that can serve as competing substrates for downstream
323 enzymes. To better validate the entire pathway, we divided it into two segments for separate
324 verification: the first segment from tryptamine and secologanin to **2**, and the second segment from
325 **2** to **9**. When tested separately, both segments showed markedly improved performance. The first
326 segment, comprising *Cr*STR, *Rv*SGD, and *Rv*YOS produced **2** (Supplementary Fig. 5). Similarly,
327 the second segment, containing *Rv*YOO, *Rv*DYR1, *Rv*CYP72A270, *Rv*CYP71D820, and
328 *Rv*11OMT, efficiently converted externally supplied **2** to **9** (Fig. 5b and Supplementary Fig. 23).
329 These results confirmed the functionality of all biosynthetic steps and suggested that pathway
330 optimization strategies, such as protein engineering of *Rv*YOS and balanced expression of pathway
331 genes, could enhance the overall production of **9**.
332
333 **Conclusion**
334 In conclusion, we have deciphered the biosynthetic pathway of reserpine in *Rauvolfia verticillata*,
335 resolving a long-standing question in natural product chemistry. The molecule's complex
336 architecture, featuring a unique C3β stereochemistry and five consecutive chiral centers,
337 exemplifies sophisticated natural product biosynthesis. Our investigation revealed the enzymatic
338 basis for C3 epimerization, which proceeds through an oxidation-reduction sequence catalyzed by
339 an FAD-dependent oxidase (*Rv*YOO) and a medium-chain dehydrogenase/reductase (*Rv*DYR1)
340 to establish the crucial C3β stereochemistry. The pathway systematically constructs the five

341 consecutive chiral centers: the first two derive from secologanin, the third and fourth are installed
342 via stereoselective reduction by *Rv*YOS, and the final stereocenter is established through
343 cytochrome P450-catalyzed hydroxylation. Notably, while chemical synthesis typically introduces
344 the methoxy group at an early stage, nature employs a distinct late-stage strategy using a P450-
345 dependent methyltransferase, highlighting the contrasting approaches between biosynthetic and
346 synthetic chemistry. This work not only provides fundamental insights into the biosynthesis of
347 complex alkaloids but also establishes a foundation for metabolic engineering efforts aimed at
348 producing reserpine and related pharmaceutically important compounds. The enzymatic tools
349 uncovered here may enable the development of chemoenzymatic approaches for accessing
350 structurally diverse alkaloids with potential therapeutic applications.
351

352 ## Methods

353 **Candidate gene cloning**
354 The full-length sequences of candidate genes were amplified from cDNA using the primers listed in
355 Supplementary Table 2 with 2 × Phanta Max Master Mix according to the manufacturer's instructions. PCR
356 products were purified and ligated into different linearized expression vectors: 3Ω1 vector (digested with BsaI),
357 and pOPINF and pOPINM vectors (both digested with HindIII-HF and KpnI-HF) using the ClonExpress® II one
358 step cloning kit. The ligation reactions were transformed into chemically competent *E. coli* DH5*α* cells
359 (AlpaLifeBio, Shenzhen, China). Transformed cells were plated on LB agar plates containing either 50 μg/mL
360 spectinomycin for 3Ω1 constructs or 50 μg/mL ampicillin for pOPINF/pOPINM constructs. Single colonies were
361 picked and cultured overnight in 3 mL selective LB medium at 37 °C with shaking at 220 rpm. Plasmids were
362 isolated and verified by Sanger sequencing. Confirmed positive strains were mixed with an equal volume of 50%
363 glycerol and stored at −80 °C as frozen stocks.
364

365 **Transformation of *Agrobacterium tumefaciens***
366 The 3Ω1 plasmids containing the full-length candidate gene were transformed into chemically competent *A.*
367 *tumefaciens* strain GV3101 (AngYuBio., Shanghai, China) following the manufacturer's instructions. The
368 transformed cells were plated onto LB agar plates containing 50 μg/mL rifampicin, 50 μg/mL gentamycin, and
369 25 μg/mL spectinomycin, and incubated at 28 °C for 2-3 days. Single colonies were picked and grown overnight
370 at 28 °C in 5 mL of LB medium containing 50 μg/mL rifampicin, 50 μg/mL gentamycin, and 25 μg/mL
371 spectinomycin. The overnight cultures were mixed with an equal volume of 50% glycerol and stored at −80 °C
372 as frozen stocks.
373

374 **Transient expression of candidate genes in *N. benthamiana***
375 *Agrobacterium* GV3101 strains harboring the constructs of candidate genes were cultivated in 3 mL LB medium
376 supplemented with 25 μg/mL rifampicin, 25 μg/ml gentamycin, and 50 μg/ml spectinomycin overnight at 28 °C
377 with a shaking of 220 rpm. The overnight cultures were centrifuged at 4,000 g for 10 min at room temperature.
378 The cell pellet was resuspended in 3 mL infiltration buffer (50 mM MES, 22.2 mM glucose, 10 mM $MgCl_2$ and
379 100 μM acetosyringone). After centrifugation at 4,000 g for 10 min, the pellet was resuspended in 5 mL
380 infiltration buffer and adjusted to an OD_{600} of 0.6. The bacterial suspension was incubated at room temperature
381 for 2 h in the dark with gentle shaking before being infiltrated into the abaxial (bottom) side of 4-week-old *N.*
382 *benthamiana* leaves using a needleless 1 mL syringe. Four days post-infiltration, substrate solutions (200 μM in
383 water or in 1 % DMSO) were infiltrated into the same areas of Agrobacterium-infiltrated leaves using a
384 needleless 1 mL syringe. Substrate-infiltrated leaves were harvested 2 days after substrate introduction for
385 metabolite analysis. Each biological replicate consisted of leaves from independent *N. benthamiana* plants (n≥3).

386
387 **Heterologous expression of candidate genes in *E. coli* BL21 (DE3)**
388 Chemically competent *E. coli* BL21 (DE3) cells (AlpaLifeBio) were transformed with pOPINF or pOPINM
389 plasmids containing the coding sequences of interest. Transformants were selected on LB agar plates
390 supplemented with 100 μg/mL ampicillin and verified by colony PCR using vector-specific sequencing primers
391 (Supplementary Table 3). For each strain, a single colony was used to inoculate 10 mL of LB medium containing
392 100 μg/mL ampicillin, which was cultured overnight at 37 °C in a temperature-controlled shaker incubator. The
393 overnight culture was then used to inoculate 400 mL of TB media with 100 μg/mL ampicillin. Cultures were
394 grown at 37 °C with a shaking of 220 rpm until reaching an OD_{600} of 0.6-0.8. At this point, the temperature was
395 lowered to 18 °C, and protein expression was induced by adding isopropyl *β*-D-1-thiogalactopyranoside (IPTG)
396 to a final concentration of 0.5 mM. After approximately 16 hours of induction, the cultures were centrifuged at
397 8,000 rpm at 4 °C for 10 min to harvest the cells.
398
399 **Protein purification**
400 Bacterial cells were resuspended in lysis buffer (100 mM Tris-HCl, 100 mM NaCl, 5% glycerol (*v/v*), pH 8.0)
401 and disrupted using a high-pressure cell disruption equipment (ATS Engineering, Suzhou, China). The remaining
402 steps were performed at 4 °C or on ice. The cell lysates were clarified by centrifugation 12,000 rpm for 30 min,
403 and the supernatant (crude enzyme) was collected. The clarified lysate was loaded onto a column packed with
404 Ni-NTA Beads 6FF agarose resin (Smart-Lifesciences). The column was washed with Tris-HCl buffer before
405 stepwise elution using increasing concentrations of imidazole (30−300 mM) in Tris-HCl buffer. Elution fractions
406 were collected separately and analyzed by sodium dodecyl sulfate polyacrylamide gel electrophoresis (SDS-
407 PAGE) with Coomassie Blue staining. Fractions containing the purified protein were combined and concentrated
408 using Amicon Ultra-15 Centrifugal Filter Units (10 kDa molecular weight cutoff) via centrifugation at 3,500
409 rpm for 1 h at 4 °C. The concentrated protein solution (<0.5 mL) underwent two rounds of buffer exchange with
410 ice-cold HEPES buffer (50 mM HEPES, pH 7.5, 100 mM NaCl) to remove imidazole. The final protein
411 preparation was diluted to approximately 2 mL with ice-cold HEPES buffer. Protein concentrations were
412 determined using a NanoDrop spectrophotometer. Aliquots of the purified protein were flash-frozen in liquid
413 nitrogen and stored at −80 °C until further use.
414
415 **Enzymatic in vitro assays**
416 Enzymatic assays for reductase activity
417 The reductase activity of recombinant *Rv*YOS was assessed using tryptamine and secologanin as substrate.
418 Reaction mixtures (100 μL total volume) contained 1 μM *CrS*TR, 1 μM *Rv*SGD, 2 μM *Rv*YOS, 100 μM NADPH,
419 25 μM tryptamine, and 25 μM secologanin in 50 mM HEPES (pH 7.4). The reactions were incubated at 30 °C
420 with shaking at 500 rpm for 8 h. The reactions were quenched by adding an equal volume of methanol, followed
421 by vacuum concentration to dryness. The residues were reconstituted in 100 μL methanol and centrifugation at
422 15,000 × g for 10 min. The supernatants were filtered through 0.22 μm PTFE syringe filters for LC-MS analysis
423 (LC-MS Method 1).
424
425 The reductase activity of recombinant *Rv*DYR1 and *Rv*DYR2 was assessed using 3-dehydro-α-yohimbine (**3**)
426 as substrate. Reaction mixtures (50 μL total volume) contained 1 μM purified reductase, 100 μM NADPH, and
427 40 μM **3** in 50 mM HEPES (pH 7.4). Reactions were incubated at 30°C with shaking at 500 rpm for 12 h. Boiled
428 enzymes (90 °C, 10 min) served as negative controls. Reactions were quenched by adding an equal volume of
429 methanol, followed by centrifugation at 15,000 × g for 10 min. The supernatants were filtered through 0.22 μm
430 PTFE syringe filters for LC-MS analysis (LC-MS Method 2).
431
432 Enzymatic assays for *O*-methyltransferase activity
433 The *O*-methyltransferase activity of recombinant *Rv*11OMT candidate was assessed using 50 μM 11,18β-
434 hydroxy-3-epi-α-yohimbine (**6**) as substrate. Reaction mixtures (50 μL total volume) contained 1 μM *Rv*11OMT,
435 250 μM *S*-adenosyl methionine (SAM), and 200 μM ascorbate in 50 mM HEPES (pH 7.4). Reactions were
436 incubated at 30 °C with shaking at 500 rpm for 12 h and quenched by adding an equal volume of methanol,
437 followed by centrifugation at 15,000 × g for 10 min. Sample preparation for LC-MS analysis was performed as
438 described above for reductase activity assays.

439
440 Enzymatic assays for UGTs activity
441 The UGT activity of recombinant *Rv*UGT1 and *Rv*UGT2 was assessed using trimethylgallic acid and UDP-
442 glucose as substrate. Reaction mixtures (100 μL total volume) contained 2 μM purified enzymes, 50 μM
443 trimethylgallic acid, and 25 μM UDP-glucose in 50 mM HEPES (pH 7.4). The reactions were treated as for
444 reductase activity assays, and analysis was performed as described in the LC-MS analysis (LC-MS Method 3).
445
446 **Heterologous expression of *Rv*CYP71D820 in *Saccharomyces cerevisiae***
447 The full-length coding sequence of *Rv*CYP71D820 and *Arabidopsis thaliana* NADPH-cytochrome P450
448 reductase (*At*CPR) were cloned into the yeast expression vector pESC-Ura under the control of GAL1 and
449 GAL10, respectively. The resulting construct was transformed into *S. cerevisiae* WAT11 chemically competent
450 cells (Coolaber, Beijing, China) using the lithium acetate/single-stranded carrier DNA/polyethylene glycol
451 (LiAc/SS carrier DNA/PEG) method as described previously[45]. Transformants were selected on synthetic
452 defined medium lacking uracil (SD-Ura). Positive clones were identified by colony PCR using vector-specific
453 primers listed in Supplementary Table 4.
454
455 Single colonies of recombinant *S. cerevisiae* strains were cultured in 10 ml of SD-Ura liquid medium containing
456 2% glucose and grown at 30 °C for 24 h with a shaking of 220 rpm. To induce protein expression, the cells were
457 harvested by centrifugation (1,000 rpm, 5 min) at room temperature and resuspended in 500 mL of SD-Ura
458 medium supplemented with 2% glucose and 1.8% galactose. The cultures were then incubated at 30 °C with a
459 shaking of 220 rpm for approximately 3-4 days. Yeast cells were harvested by centrifugation (1,000 g, 5 min)
460 for microsomal protein preparation.
461
462 **Preparation of *Rv*CYP71D820-containing microsome**
463 Isolation of yeast microsomal protein followed a previously described protocol[46]. The cell pellet was
464 resuspended in TEK buffer (50 mM Tris-HCl, 1 mM EDTA, 100 mM potassium chloride, pH 7.4) at a ratio of
465 1 mL buffer per 0.5 g wet cell pellet mass and incubated at room temperature for 5 min. Cells were harvested by
466 centrifugation (1,000 g, 5 min) and then resuspended in 50 mL ice-cold TES B buffer (50 mM Tris-HCl, 1 mM
467 EDTA, 600 mM sorbitol, pH 7.4). The cell suspensions were lysed using an ultra-high-pressure homogenizer
468 (1100 bar, 5 min, 4 °C). Cell debris was removed by centrifugation (10,000 g, 15 min, 4 °C). The supernatant
469 was further centrifuged at 87,000 × g for 60 min at 4 °C. The resulting microsomal pellet was resuspended in 2
470 mL of ice-cold TEG buffer (50 mM Tris-HCl, 1 mM EDTA, 20% [*v/v*] glycerol, pH 7.4). The protein
471 concentration in the microsomal fraction was measured using the Bio-Rad Protein Assay Kit. Aliquots (100 μL)
472 were snap-frozen in liquid nitrogen and stored at −80 °C until further use.
473
474 ***In vitro* assays of *Rv*CYP71D820**
475 The enzymatic activity of *Rv*CYP71D820 was assessed in a reaction mixture (100 μL final volume) containing
476 40 μM substrate, 2 mM NADPH, 50 mM phosphate buffer (pH 8.0), and 30 μL microsomal fraction. The reaction
477 mixture was incubated at 30 °C for 16 h. Reactions were terminated by the addition of 200 μL methanol. The
478 reaction mixture was concentrated to dryness using a vacuum concentrator (Eppendorf, Hamburg, Germany) at
479 30 °C. The residue was redissolved in 100 μL methanol and subjected to analysis.
480
481 **Metabolite extraction**
482 For *R. serpentina* tissue analysis, freeze-dried tissue was ground to a fine powder, and 10 mg was accurately
483 weighed into a microcentrifuge tube. The tissue was extracted with 300 μL methanol in an ultrasonic bath (SB-
484 3200DT, Scientz, Ningbo, China) at room temperature for 30 min. The extracts were centrifuged at 15,000 rpm
485 for 5 min at room temperature, and the supernatant was filtered through a 0.22 μm PES syringe filter into HPLC
486 vials for analysis.
487
488 For *Nicotiana benthamiana* samples, leaves were collected with a 1.0-cm diameter cork borer. The leaf discs
489 were transferred to 2 mL microcentrifuge tubes and lyophilized overnight in a freeze dryer (SCIENTZ-10N,
490 Ningbo Scientz Biotechnology Co., Ltd). The dried tissue was extracted with 600 μL methanol and homogenized

using a homogenizer (SWE-D6, Servicebio, Hubei, China). The homogenate was centrifuged at 15,000 rpm for 10 min, and the supernatant was filtered through a 0.22 μm PES syringe filter into HPLC vials for analysis.

HPLC analysis and purification

Analytical high performance liquid chromatography (HPLC) was performed on an Agilent 1260 Series liquid chromatography system equipped with a multiple wavelength detector and a COSMOSIL 5C18-MS-II column (250 mm × 4.6 mm, 5 μm particle size). The injection volume was 10 μL and the flow rate was 1.0 mL/min using 0.1% formic acid in water as mobile phase A and acetonitrile as mobile phase B. Samples were analyzed with the following liquid chromatography gradient: 0-5 min, 10% B isocratic; 5-25 min, 10% to 50% B; 25-30 min, 50% to 95% B;30-40 min, 10% B isocratic.

Semi-preparative HPLC was carried out using the same Agilent 1260 Series system equipped with either a COSMOSIL 5C18-MS-II column (250×10 mm, 5 μm particle size) or an XBridge BEH C18 OBD Prep column (250 mm ×10 mm, 5 μm particle size, , 130Å pore size). The injection volume was 50 μL and the follow rate was 3 mL/min using 0.1% formic acid in water as mobile phase A and acetonitrile as mobile phase B. For compound isolation, the following liquid chromatography gradient was applied: 0-10 min, 10% B isocratic; 10-40 min, 10% to 50% B; 40-50 min, 50% to 95% B; 50-60 min, 10% B isocratic. The fractions were collected based on UV absorption at 254 nm.

LC-MS analysis

Method 1

Liquid chromatography-mass spectrometry (LCMS) analysis was performed using a SIL-30AC HPLC system (SHIMADZU, Kyoto, Japan) coupled to a ZenoTOF 7600 System (Ultra-High-Resolution Quadrupole-Time-of-Flight) mass spectrometer (AB SCIEX, Framingham, MA, USA). Chromatographic separation was achieved using a Phenomenex Kinetex XB-C18 column (100 mm × 2.1 mm, 1.7 μm particle size; 100 Å pore size) maintained at 40 °C. The injection volume was 3 μL and the flow rate was 0.3 mL/min using 0.1 % formic acid in water as mobile phase A and acetonitrile as mobile phase B. Authentic standards were prepared in methanol at concentrations ranging from 20-100 μM. The liquid chromatography gradient elution program was as follows: 0-5 min, 5 % B isocratic; 5-15 min, 5 % B to 50 % B; 15-20 min, 50 % B to 95 % B; 20-22 min, 95 % B isocratic; 22-25 min, 5 % B isocratic. Mass spectrometry was performed in positive electrospray ionization mode using data-independent acquisition (DIA). Operating parameters were as follows: capillary voltage, 3500 V; end plate offset, 500 V; nebulizer pressure, 2.5 bar; drying gas (N_2) temperature, 250 °C; drying gas flow rate, 11 L/min. Mass spectra were acquired over the range *m/z* 50 to 1000. For MS/MS analysis, fragmentation was triggered at an absolute threshold of 100 with a total cycle time of 0.3-0.5 s and collision energy of 35 eV.

Method 2

Additional LC-MS analysis was performed using a Vanquish liquid chromatography system (Thermo Fischer Scientific) connected to an IMPACT II System (High Resolution Quadrupole-Time-of-Flight) mass spectrometer (Bruker). Separation was achieved using a Waters Acquity BEH C18 column (100 mm × 2.1 mm, 2.5 μm particle size) operated at 40 °C with a flow rate of 0.3 mL/min and injection volume of 3 μL. The mass spectrometry was operated in positive electrospray ionization mode (ESI^+) with the following parameters: capillary voltage, 3500 V; end plate offset, 500 V; nebulizer pressure, 2.5 bar; drying gas (N_2) temperature, 250 °C; drying gas flow rate, 8 L/min. Data acquisition was performed in autoMS/MS mode at 12 Hz over *m/z* 50-1000. Fragmentation was triggered on an absolute threshold of 500 with a cycle time of 0.5 s. Collision energy was applied using a stepping gradient either from 11.0 to 44.0 eV or from 35.0 to 52.5 eV.

Method 3

Additional LC-MS analysis was performed using a Vanquish liquid chromatography system (Thermo Fischer Scientific) connected to an IMPACT II System (High Resolution Quadrupole-Time-of-Flight) mass spectrometer (Bruker). Separation was achieved using a Waters Acquity BEH C18 column (100 mm × 2.1 mm, 2.5 μm particle size) operated at 40 °C with a flow rate of 0.3 mL/min and injection volume of 3 μL. The mass spectrometry was operated in positive electrospray ionization mode (ESI^-) with the following parameters: capillary voltage, 4000 V; end plate offset, 500 V; nebulizer pressure, 2.5 bar; drying gas (N_2) temperature,

250 °C; drying gas flow rate, 8 L/min. Data acquisition was performed in autoMS/MS mode at 12 Hz over *m/z* 50-1000. Fragmentation was triggered on an absolute threshold of 500 with a cycle time of 0.5 s. Collision energy was applied using a stepping gradient from 17.5 to 35 eV.

Data availability

The gene sequences of all characterized enzymes are provided in Supplementary Table 1. The transcriptome data generated in this study have been deposited in the National Genomics Data Center BioProject databased with the accession number PRJCA035431.

References

1. Müller, J. M., Schlittler, E. & Bein, H. J. Reserpin, der sedative Wirkstoff aus *Rauwolfia serpentina* Benth. *Experientia* 8, **338** (1952).

2. Carlsson, A., Lindqvist, M. & Magnusson, T. 3,4-Dihydroxyphenylalanine and 5-hydroxytryptophan as reserpine antagonists. *Nature* **180**, 1200 (1957).

3. Brodie, B. B., Olin, J. S., Kuntzman, R. G. & Shore, P. A. Possible interrelationship between release of brain norepinephrine and serotonin by reserpine. *Science* **125**, 1293-1294 (1957).

4. Vakil, R. J. *Rauwolfia serpentina* in the treatment of high blood pressure: a review of the literature. *Circulation* **12**, 220-229 (1955).

5. Braslow, J. T. & Marder, S. R. History of Psychopharmacology. *Annu. Rev. Clin. Psychol*. **15**, 25-50 (2019).

6. Carlsson, A. A paradigm shift in brain research. *Science* **294**, 1021-1024 (2001).

7. Chen, F. -E. & Huang, J. Reserpine: a challenge for total synthesis of natural products. *Chem. Rev*. **105**, 4671-4706 (2005).

8. Woodward, R. B. et al. The total synthesis of reserpine. *J. Am. Chem. Soc*. **78**, 9, 2023-2025 (1956).

9. Chu, C. -S., Liao, C. -C. & Rao, P. D. A formal synthesis of (±)-reserpine from methyl vanillate. *Chem. Commun*. 1537-1538 (1996).

10. Mehta, G. & Reddy, D. S. A formal synthesis of reserpine: hydrindane approach to the Woodward's ring-E precursor. *J. Chem. Soc. Perkin Trans*. **1**, 1399-1404 (2000).

11. Stork, G. The stereospecific synthesis of reserpine. *Pure Appl. Chem*. **61**, 439-442 (1989).

12. Gomez, A. M., Lopez, J. C. & Fraser-Reid, B. Serial radical cyclization of pyranose-derived dienes in the stereocontrolled synthesis of densely functionalized cyclohexanes. A route to Woodward's reserpine precursor. *J. Org. Chem*. **59**, 4048-4050 (1994).

577 13. Leete, E. The Biogenesis of the Rauwolfia alkaloids. I. The incorporation of tryptophan into
578 ajmaline. *J. Am. Chem. Soc*. **82**, 6338-6342 (1960).

579 14. Battersby, A. R., Burnett, A. R. Parsons, P. G. Alkaloid biosynthesis. Part XV. Partial
580 synthesis and isolation of vincoside and isovincoside: biosynthesis of the three major classes of
581 indole alkaloids from vincoside. *J. Chem. Soc. C* 1193-1200 (1969).

582 15. O'Connor, S. E. & Maresh, J. J. Chemistry and biology of monoterpene indole alkaloid
583 biosynthesis. *Nat. Prod. Rep*. **23**, 532-547 (2006).

584 16. Gerasimenko, I., Sheludko, Y., Unger, M. & Stöckigt, J. Development of an efficient system
585 for the separation of indole alkaloids by high performance liquid chromatography and its
586 applications. *Phytochem. Anal*. **12**, 96-103 (2001).

587 17. Gerasimenko, I. et al. Heterologous expression of a *Rauvolfia* cDNA encoding strictosidine
588 glucosidase, a biosynthetic key to over 2000 monoterpene indole alkaloids. *Eur. J. Biochem*. **269**,
589 2204-2213 (2002).

590 18. Yerkes, N. et al. Substrate specificity and diastereoselectivity of strictosidine glucosidase, a
591 key enzyme in monoterpene indole alkaloid biosynthesis. *Bioorg. Med. Chem. Lett*. **18**, 3095-3098
592 (2008).

593 19. Zhan, G. et al. Monoterpene indole alkaloids with diverse skeletons from the stems of
594 *Rauvolfia vomitoria* and their acetylcholinesterase inhibitory activities. *Phytochemistry* **177**,
595 112450 (2020).

596 20. Falkenhagen, H. et al. Indole alkaloids from "hairy roots" of *Rauwolfia serpentina. Can. J.*
597 *Chem.* **71***,* 2201-2203 (1993).

598 21. Kumar, S., Kumari, D. & Singh, B. Genus *Rauvolfia*: A review of its ethnopharmacology,
599 phytochemistry, quality control/quality assurance, pharmacological activities and clinical evidence.
600 *J. Ethnopharmacol*. **295**, 115327 (2022).

601 22. Stander, E. A. et al. The *Rauvolfia tetraphylla* genome suggests multiple distinct biosynthetic
602 routes for yohimbine monoterpene indole alkaloids. *Commun. Biol*. **6**, 1197 (2023).

603 23. Chen, R. et al. Molecular cloning and characterization of the strictosidine synthase gene
604 from *Rauwolfia verticillata*. *Russ. J. Plant Physiol*. **55**, 670–675 (2008).

605 24. Xu, H. et al. Cloning and characterization of the strictosidine-β-D-glucosidase (SGD) gene
606 from *Rauvolfia verticillata*. *Agric. Sci. Technol*. **13**, 1406-1409 (2012).

607 25. Allard, S. T., Giraud, M. F. & Naismith, J. H. Epimerases: structure, function and mechanism.
608 *Cell Mol. Life Sci*. **58**, 1650-1665 (2001).

609 26. Garg, A. et al. Elucidation of the cryptic epimerase activity of redox-inactive ketoreductase
610 domains from modular polyketide synthases by tandem equilibrium isotope exchange. *J. Am.*
611 *Chem. Soc*. **136**, 10190-10193 (2014).

612 27. Farrow, S. C., Hagel, J. M., Beaudoin, G. A. W., Burns, D. C. & Facchini, P. J. Stereochemical
613 inversion of (*S*)-reticuline by a cytochrome P450 fusion in opium poppy. *Nat. Chem. Biol*. **11**, 728-
614 732 (2015).

615 28. Caputi, L. et al. Missing enzymes in the biosynthesis of the anticancer drug vinblastine in
616 Madagascar periwinkle. *Science* **360**, 1235-1239 (2018).

617 29. Langley, C. et al. Expansion of the catalytic repertoire of alcohol dehydrogenases in plant
618 metabolism. *Angew. Chem. Int. Ed. Engl*. **61**, e202210934 (2022).

619 30. Trenti, F. et al. Early and late steps of quinine biosynthesis. *Org. Lett*. **23**, 1793-1797 (2021).

620 31. Schotte, C. et al. Directed biosynthesis of mitragynine stereoisomer. *J. Am. Chem. Soc.* **145**,
621 4957-4963 (2023).

622 32. Kim, K. et al. Biosynthesis of kratom opioids. *New Phytol*. **240**, 757-769 (2023).

623 33. Stavrinides, A. et al. Unlocking the diversity of alkaloids in *Catharanthus roseus*: nuclear
624 localization suggests metabolic channeling in secondary metabolism. *Chem. Biol*. **22**, 336-341
625 (2015).

626 34. McDonald, A. et al. Enzymatic epimerization of monoterpene indole alkaloids in Kratom.
627 bioRxiv 2024.12.13.628308; doi: https://doi.org/10.1101/2024.12.13.628308.

628 35. Hwang, J. et al. Ancient gene clusters initiate monoterpene indole alkaloid biosynthesis and C-
629 3 stereochemistry inversion. bioRxiv 2025.01.07.631695. doi: https://doi.org/10.1101/
630 2025.01.07.631695.

631 36. Besseau S. et al. A pair of tabersonine 16-hydroxylases initiates the synthesis of vindoline in
632 an organ-dependent manner in *Catharanthus roseus*. *Plant Physiol*. **163**, 1792-1803 (2013).

633 37. St-Pierre, B. & De Luca, V. A Cytochrome P450 monooxygenase catalyzes the first step in the
634 conversion of tabersonine to vindoline in *Catharanthus roseus*. *Plant Physiol*. **109**, 131-139 (1995).

635 38. Levac, D., Murata, J., Kim, W. S. & De Luca, V. Application of carborundum abrasion for
636 investigating the leaf epidermis: molecular cloning of *Catharanthus roseus* 16-
637 hydroxytabersonine-16-*O*-methyltransferase. *Plant J*. **53**, 225-236 (2008).

638 39. Murata, J., Roepke, J., Gordon, H. & De Luca, V. The leaf epidermome of *Catharanthus roseus*
639 reveals its biochemical specialization. *Plant Cell* **20**, 524-542 (2008).

640 40. Schneider, J. A. et al. Pharmacological studies with deserpidine, a new alkaloid from *Rauwolfia*
641 *canescens*. *J. Pharmacol. Exp. Ther*. **114**, 10-13 (1955).

642 41. Lam, K. C., Ibrahim, R. K., Behdad, B. & Dayanandan, S. Structure, function, and evolution
643 of plant *O*-methyltransferases. *Genome* **50**, 1001-1013 (2007).

644 42. Bontpart, T., Cheynier, V., Ageorges, A. & Terrier, N. BAHD or SCPL acyltransferase? What

645 a dilemma for acylation in the world of plant phenolic compounds. *New Phytol*. **208**, 695-707
646 (2015).

647 43. Li, P. et al. Multiomics analyses of two *Leonurus* species illuminate leonurine biosynthesis
648 and its evolution. *Mol. Plant* **17**, 158-177 (2024).

649 44. Zhao, Y. et al. Flavano-3-ol galloylation-related functional gene cluster and the functional
650 diversification of *SCPL* paralogs in *Camellia* sp. *J. Agric. Food Chem*. **71**, 488-498 (2023).

651 45. Gietz, R. D. &Woods, R. A. Transformation of yeast by lithium acetate/single-stranded carrier
652 DNA/polyethylene glycol method, *Method. Enzymol.* **350**, 87-96 (2002).

653 46. Pompson, D., Louerat, B., Bronine, A. & Urban, P. Yeast expression of animal and plant P450s
654 in optimized redox environments. *Methods Enzymol*. **272**, 51-64 (1996).
655

656 **Acknowledgements**

657 We thank Dr. David Nelson (University of Tennessee) for his assistance with naming
658 *Rv*CYP72A270 and *Rv*CYP71D820 identified in this study. We are grateful to the Shenzhen
659 Synthetic Biology Infrastructure for instrument support and technical assistance. This research was
660 supported by the National Key R&D Program of China (2023YFA0915500) and Shenzhen Science
661 and Technology Program (KJZD20230923115906013) to Y. J, National Natural Science
662 Foundation of China (82104023) to J. C.
663

664 **Author contributions**

665 J. C., J. Z, and F. L. performed the experiments and analyzed the data. J. C. and Y. J. designed the
666 experiments, wrote and revised the manuscript. Y. J. supervised the project. All authors discussed
667 the results and commented on the manuscript.
668

669 **Competing interests**

670 The authors declare no competing interests.
671
672
673
674
675
676

Fig. 1: Structural features, synthetic history, and biosynthetic pathway of reserpine.

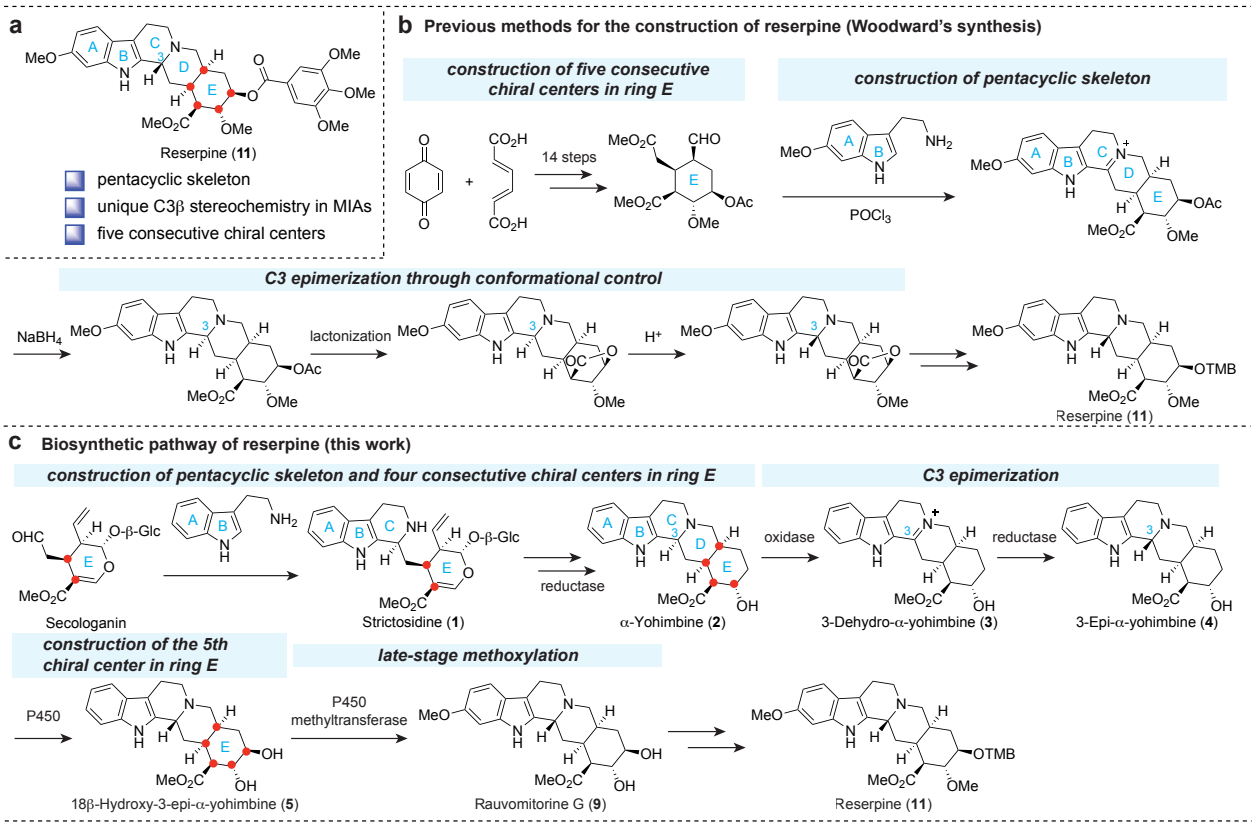

a, Chemical structure of reserpine (**11**) highlighting its key structural features. **b**, Previous synthetic approaches exemplified by Woodward's synthesis. **c**, The biosynthetic pathway of reserpine identified in this work. TMB represents 3,4,5-trimethoxybenzoyl group.

694 **Fig. 2: The biosynthetic pathway of reserpine in *R. verticillata*.**

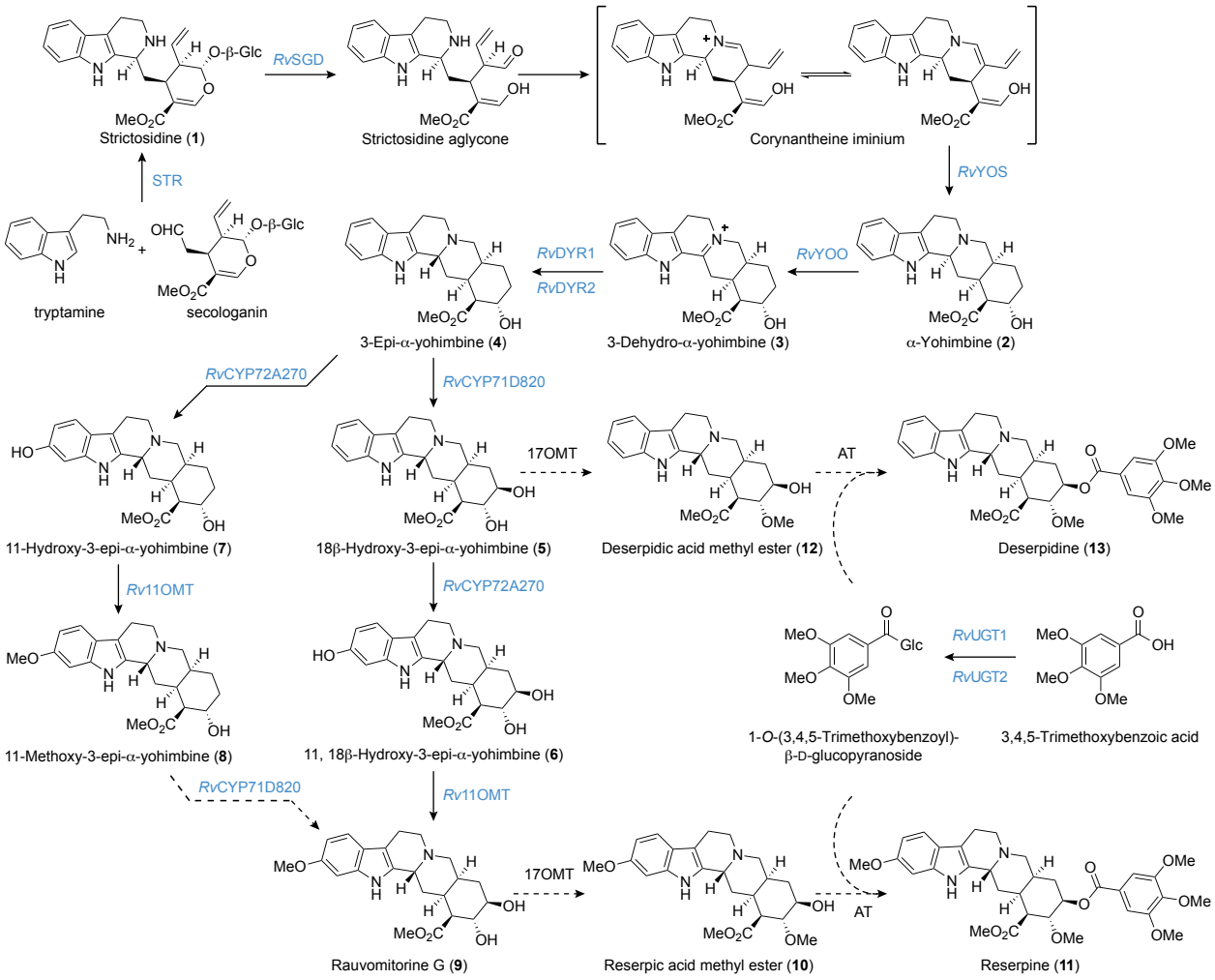

695

696 Solid arrows indicate characterized steps; dashed arrows indicate proposed steps. Names of
697 characterized enzymes are shown in blue. AT represents acyltransferase.

698

699

700

701

702

703

704

705

Fig. 3: Identification and characterization of enzymes involved in α-yohimbine epimerization.

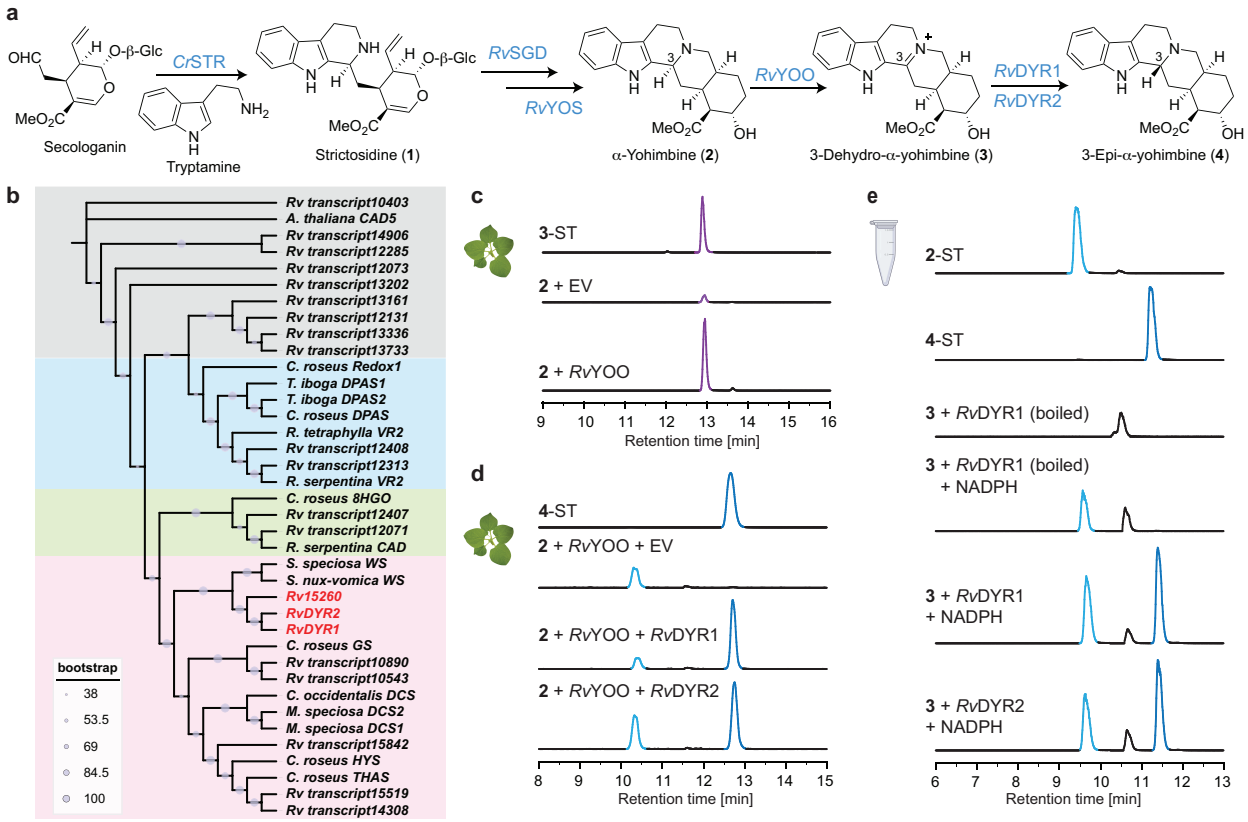

a, Proposed biosynthetic pathway from tryptamine and secologanin to 3-epi-α-yohimbine (**4**) via α-yohimbine (**2**) and 3-dehydro-α-yohimbine (**3**) intermediates. **b**, Phylogenetic analysis of medium-chain dehydrogenase/reductase (MDR) enzymes, with colored boxes indicating different reaction types catalyzed by characterized enzymes. Bootstrap values are shown as circles of varying sizes. **c**, LC-MS analysis showing oxidation of α-yohimbine (**2**) by *Rv*YOO expressed in *N. benthamiana* leaves compared to empty vector (EV) control and standard (ST) of **3**. **d**, LC-MS analysis demonstrating conversion of α-yohimbine (**2**) to 3-epi-α-yohimbine (**4**) by co-expression of *Rv*YOO with *Rv*DYR1 or *Rv*DYR2 in *N. benthamiana*. **e**, In vitro characterization of purified *Rv*DYR1 and *Rv*DYR2 showing stereoselective reduction of synthetic 3-dehydro-α-yohimbine (**3**) to 3-epi-α-yohimbine (**4**) in the presence of NADPH.

Fig. 4: Discovery and characterization of enzymes responsible for C11 and C18 hydroxylation and *O*-methylation.

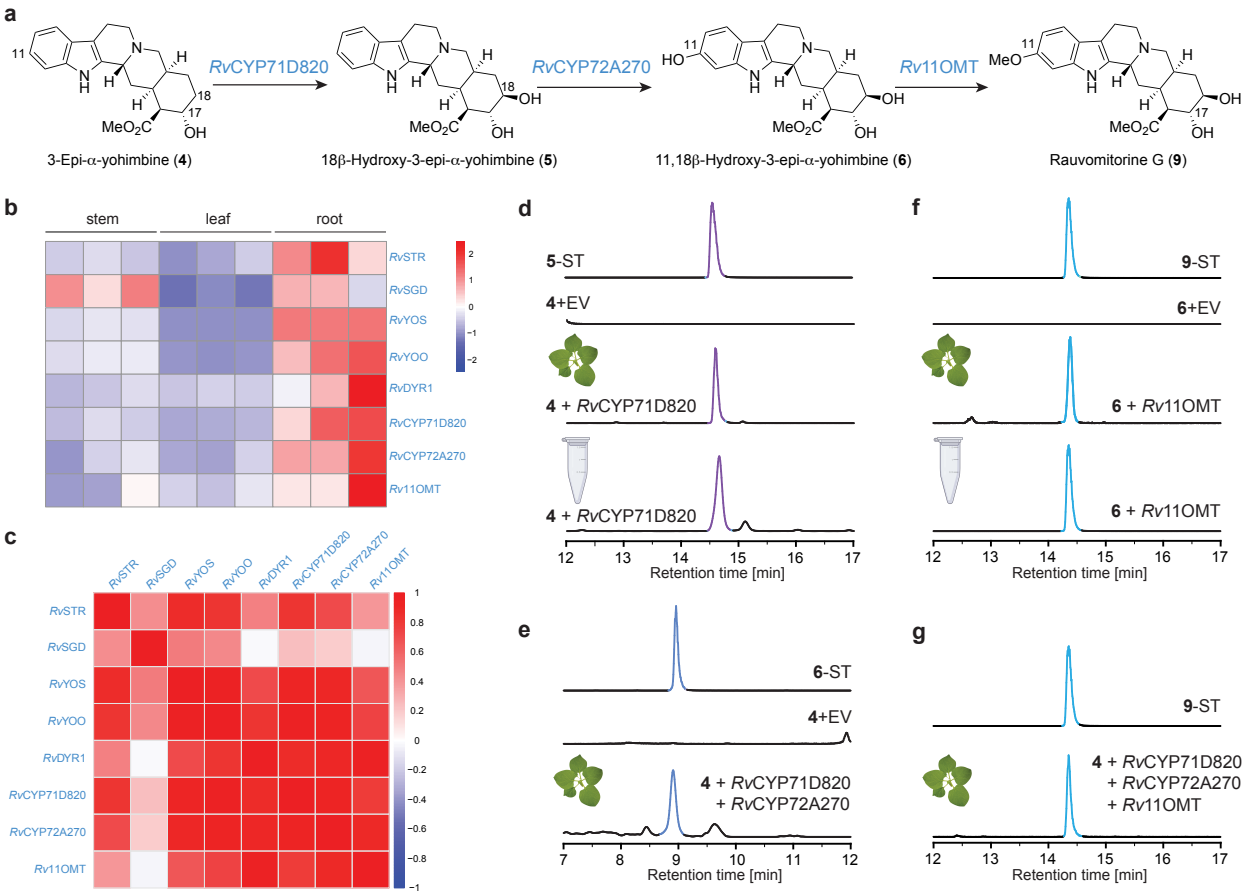

a, Proposed biosynthetic pathway from 3-epi-α-yohimbine (**4**) to rauvomitorine G (**9**) via sequential hydroxylation and *O*-methylation reactions. **b**, Tissue-specific expression patterns of biosynthetic genes in *R. verticillata* stem, leaf, and root tissues; **c**, Correlation matrix showing Pearson correlation coefficients between expression levels of identified biosynthetic genes. **d**, LC-MS analysis of *Rv*CYP71D820-catalyzed C18 hydroxylation of **4** in *N. benthamiana* (leaf icon) and *in vitro* using yeast microsomes (tube icon), compared with synthetic standard of **5**. **e**, LC-MS analysis showing formation of 11,18β-dihydroxy-3-epi-α-yohimbine (**6**) through co-expression of *Rv*CYP71D820 and *Rv*CYP72A270 *in N. benthamiana*, compared with synthetic standard of **6**. **f**, LC-MS analysis of *Rv*11OMT-catalyzed *O*-methylation of **6** in *N. benthamiana* and *in vitro* using purified enzyme, compared with synthetic standard of **9**. **g**, LC-MS analysis of the reconstitution of **9** from **4** through co-expression of *Rv*CYP71D820, *Rv*CYP72A270, and *Rv*11OMT in *N. benthamiana*. EV, empty vector control; ST, synthetic standard.

Fig. 5: Reconstitution of rauvomitorine G biosynthesis.

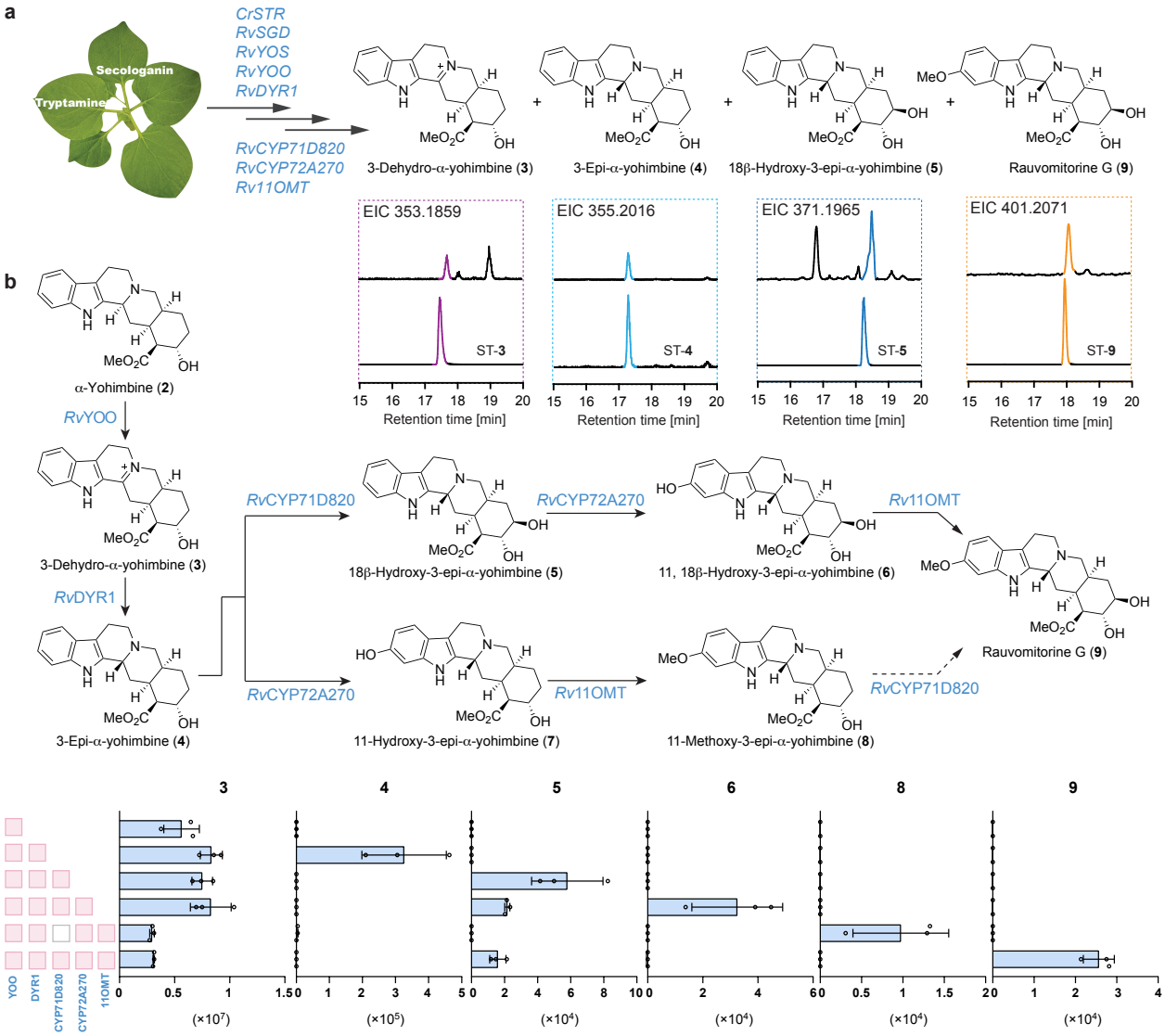

a, Reconstitution of the complete biosynthetic pathway in tobacco using eight enzymes with tryptamine and secologanin as substrates. Extracted ion chromatograms (EIC) show the detection of intermediates **3**, **4**, **5** and final product **9**. **b**, Stepwise reconstitution and validation of the biosynthetic pathway from α-yohimbine (**2**) to rauvomitorine G (**9**), showing the sequential enzymatic transformations and corresponding intermediates. Bar graphs indicate peak areas of pathway intermediates (n = 3 biological replicates, error bars represent standard deviation).